1-11-2012

# Random Vs Regularized OPV: Limits of Performance Gain of Organic Bulk Heterojunction Solar Cells by Morphology Engineering

Biswajit Ray
*Purdue University - Main Campus*, ray0@purdue.edu

Muhammad A. Alam
*Birck Nanotechnology Center, Purdue University*



Ray, Biswajit and Alam, Muhammad A., "Random Vs Regularized OPV: Limits of Performance Gain of Organic Bulk Heterojunction Solar Cells by Morphology Engineering" (2012). *Birck and NCN Publications.* Paper 854.
http://dx.doi.org/10.1016/j.solmat.2011.11.042

Solar Energy Materials & Solar Cells 99 (2012) 204–212

Contents lists available at SciVerse ScienceDirect

Solar Energy Materials & Solar Cells

journal homepage: www.elsevier.com/locate/solmat

# Random vs regularized OPV: Limits of performance gain of organic bulk heterojunction solar cells by morphology engineering

Biswajit Ray*, Muhammad A. Alam

*School of Electrical and Computer Engineering, Purdue University, West Lafayette, IN 47906, USA*

ARTICLE INFO

*Article history:*
Received 18 September 2011
Received in revised form
22 November 2011
Accepted 24 November 2011
Available online 4 January 2012

*Keywords:*
Organic bulk heterojunction solar cell
Solution processing
Planar heterojunction
Optimum morphology

ABSTRACT

Inexpensive solution processing of bulk heterojunction (BHJ) type organic photovoltaic (OPV) cells offers an attractive option for the low cost solar energy conversion. Solution processing creates a disordered morphology consisting of two organic semiconductors, intermixed randomly within the light-absorbing layer of the cell. In this paper, we use a detailed three-dimensional process-device co-modeling framework to show that in spite of the inherent structural randomness of the morphology, *the efficiency of solution-processed BHJ cells is nearly optimal – close to those of the perfectly ordered structures*. In addition, we show that the morphological randomness by itself does not increase the performance variability of large-area cells. Both the results indicate that the inexpensive solution processing of BHJ cells imposes no inherent limitation on the performance/variability and the ultimate efficiency of such solution-processed films should compare favorably to the other ordered OPV cells fabricated by more expensive techniques. Finally, we explore the theoretical optimum morphology for BHJ cells and find that fill factor is the only parameter through which efficiency can be enhanced by morphology engineering. We conclude by exploring the performance gains/limits of organic solar cells with the improvement in transport parameters.

Published by Elsevier B.V.

## 1. Introduction and background

Since the invention of planar heterojunction (PHJ) based organic solar cells [1], the efficiency of organic photovoltaic (OPV) technology has improved continuously, and currently it exceeds 8% for bulk heterojunction (BHJ) OPV[2]. The PHJ cells consist of a simple two layer stacked structure of donor (D) and acceptor (A) type organic semiconductors (Fig. 1a). The innovation of such stacked structure (or heterojunction) facilitated the efficient dissociation of photo-generated excitons at the planar D–A interface. However, the short circuit current density ($J_{SC}$) of PHJ cell is low, primarily because most of the photo-generated excitons self-recombine before being harvested by the D/A heterointerface. In fact, only those excitons generated within a diffusion length ($L_{ex} \sim 10$ nm) from the planar HJ can contribute to photo-current (see Fig. 1a). This problem of poor exciton collection (or low $J_{SC}$) was later solved by the bulk heterojunction (BHJ) morphology [3], where the junction between the donor and acceptor materials is distributed randomly throughout the volume of the cell, see Fig. 1b. Regardless the point of photo-excitation, this distributed D/A junction can harvest excitons efficiently, and hence BHJ–OPV cells have high $J_{SC}$. Unfortunately, the BHJ–OPV suffers from higher recombination [4] of the photo-generated carriers at the increased donor/acceptor interfacial area. Thus, even though BHJ solar cells have achieved close to 100% internal quantum efficiency for $J_{SC}$ [5], the interfacial recombination loss reduces its open circuit voltage ($V_{oc}$) and the fill factor (*FF*) significantly.

Many groups [6–10] have explored in great detail the transport and recombination of excitons, electrons and holes in BHJ solar cells by numerical simulations. These studies confirm that the performance of the BHJ–OPV is strongly correlated with the underlying morphology. However, a statistical analysis of the performance of BHJ cells as a function of the degree of randomness of its morphology has not been reported in the literature. Thus, despite many recent reports of performance gains of ordered heterojunction OPV (OHJ-OPV, see Fig. 1c) cells fabricated by various top–down approaches (e.g., nano-imprint, templating, etc.) [11–13], it is fair to ask if one could achieve similar performance gain by optimizing the inexpensive solution based fabrication process [14–17]. Indeed, there is no convincing theoretical/numerical argument to show that the intrinsic random morphology of BHJ–OPV must necessarily lead to inferior performance compared to OHJ–OPV created by sophisticated fabrication methods. There is also very little discussion regarding the performance variability of the solution-processed BHJ cells

* Corresponding author.
*E-mail addresses:* biswajit.025@gmail.com (B. Ray), alam@purdue.edu (M.A. Alam).

0927-0248/$ - see front matter Published by Elsevier B.V.
doi:10.1016/j.solmat.2011.11.042

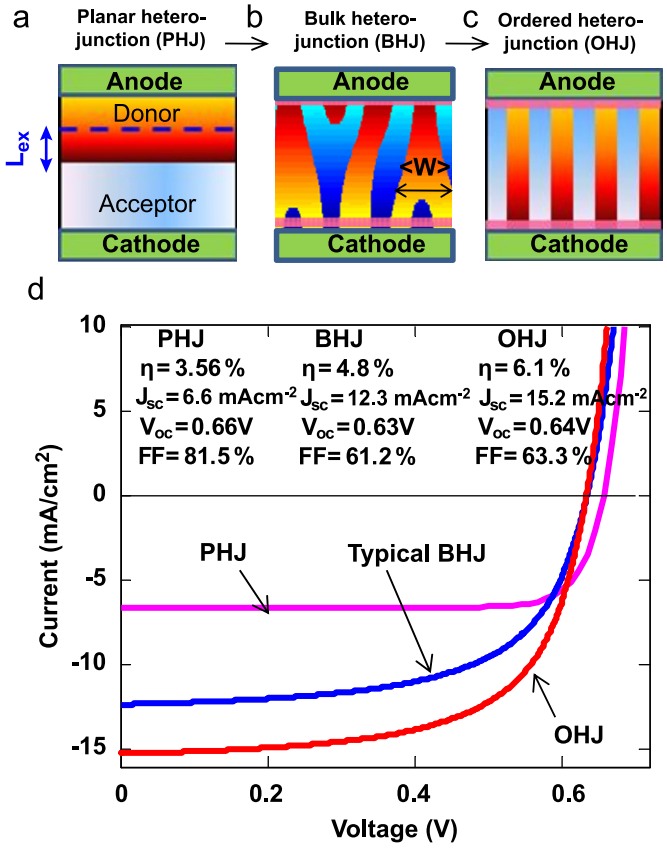


**Fig. 1.** Structures of various organic solar cells. (a) Planar heterojunction (PHJ), (b) Bulk heterojunction (BHJ), and (c) ordered heterojunction (OHJ) OPV cell in the chronological order of development. (d) Comparison of typical *J–V* characteristics for various OPV geometries.

originating from the inherent structural randomness and the implications of such variability for large-area modules. A systematic understanding and statistical analysis of such variability are important to predict/improve the panel efficiency of series-connected cells [18]. Finally, even though there are several recent works on the optimum geometry for OPVs [19–21], it remains unclear if such structures provide significant efficiency gain over that of random BJH-OPV (for comparable transport/recombination parameters). In the absence of such explicit comparison, it is difficult to predict the circumstances for which engineering ordered morphology may be appropriate.

In this paper, we address the above mentioned issues through a computational framework (based on transport simulation of excitons, electrons and holes) which connects the morphology of an OPV to its efficiency. We have four major conclusions: (1) We find that the regularization of BHJ morphology does not improve the OPV efficiency significantly. Instead, we show that efficiency of random BHJ cells, fabricated by inexpensive solution-based processing (with optimum mixing ratio and anneal duration), is close to that of the perfectly ordered structures. (2) We also demonstrate that even though the morphology of BHJ cells is inherently random, this *intrinsic* structural randomness does not affect the performance of large-area cells. However, precise control of various process parameters related to *extrinsic* variability remains a significant concern. (3) Next, we show that instead of the fully ordered structure (Fig.1c), a fin-like geometry (Fig. 4a), whose dimensions have been optimized for a given combination of material parameters, offers the highest efficiency. (4) Finally, we explain how the transport parameters affect OPV efficiency, and we find the limits of efficiency enhancement by improving the transport parameters like mobility, exciton diffusion length, etc.

The paper is organized as follows: We first describe the process and device modeling approach used in this analysis. Then we present a detailed comparison between the performance of ordered and random BHJ cells. Next we discuss the performance variability of BHJ cells due to its morphological randomness. Finally, we formulate the design rules for the optimal morphology and discuss the performance gain/limit with the improvement of various transport parameters like exciton diffusion length, charge carrier mobility, etc.

## 2. Process device co-modeling of BH–OPV

In order to explore the effect of bulk heterojunction morphology on the device performance, we first simulate the random BHJ morphology by the phase field approach. Specifically, we use the Flory–Huggins free-energy formulation within the Cahn–Hilliard transport model [22] to describe the spinodal decomposition of the respective donor–acceptor organic semiconductors. The details of the process model equations and the model parameters [23,24] are summarized in Tables 1 and 2. More sophisticated phase-field models and kinetic Monte Carlo approaches [8] have also been used by many groups to describe the finer features of the morphology. Since our goal is to explore the generic impact of morphology on efficiency of OPV cell, a simpler description of phase segregation based on the Cahn–Hilliard model, analogous to those used in Ref. [6,7], is adopted. Once the morphology is simulated, it is characterized by an average domain size [25], *W*, as shown in Fig. 2a. Unlike the BHJ morphology, the planar heterojunction (PHJ) and the ordered heterojunction (OHJ) structures are simulated not from a process model, but with fixed geometrical dimensions associated with the top–down fabrication process.

The transport of carriers (excitons, electrons, and holes) on the simulated morphology is modeled by the drift–diffusion formalism (see Eqs. (3–10) in Table 1). Optical absorption is considered only in the donor material, as is typical for P3HT:PCBM based system [26]. However, the key conclusions will not change if both donor and acceptor absorb photons. The absorption profile is assumed uniform with an effective exciton generation rate in the donor material (details on absorption profile are described in [26,27]). We then solve the steady state exciton diffusion equation in the distributed donor regions. We assume that the efficiency of exciton dissociation at the donor–acceptor hetero-interface is very high and is independent of field at the interface [28,29], so that the exciton concentration at the D–A boundary can be set to zero regardless the operating conditions. In recent years, the model for exciton transport has been generalized to include hopping transport and more complex dissociation dynamics [30], but we adopt a simpler semi-classical approach for this first discussion regarding the efficiency/variability of BHJ–OPV due to the randomness in the morphology.

The solution of exciton transport equation gives the exciton dissociation flux at the D–A interface, which we use as the charge carrier generation term in the electron and hole continuity equations [6,7]. The recombination term in the continuity equations is implemented to reflect a bi-molecular recombination process at the D/A interface [31]. Even though there is a debate in the literature regarding the dominant recombination mechanism at the hetero-interface [32], the key conclusions in the paper do not depend sensitively on the details of the recombination mechanism. Since the D–A interface is the only region where free carriers can be generated from excitons and the free

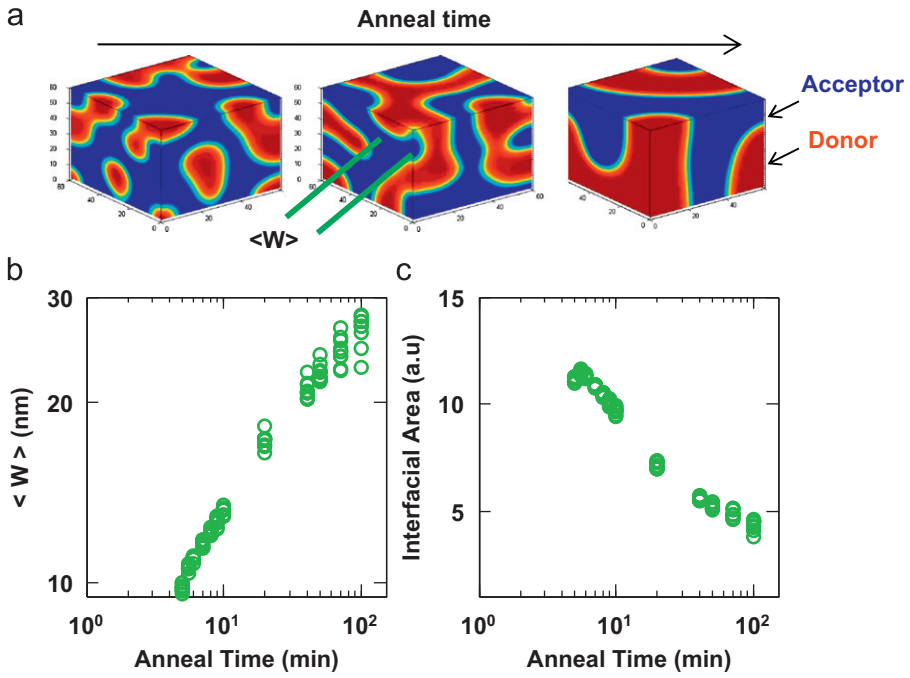


**Fig. 2.** Morphology evolution with anneal duration. (a) Three distinct morphologies of the active layer are plotted with increasing anneal duration. For clarity, the metal electrodes and the blocking layers of the complete cell have not been shown. (b) The average cluster size ($W$) of the simulated morphologies are plotted with anneal time (log–log plot). (c) Interfacial area of the 3D morphologies are plotted with anneal duration.

electron/holes can recombine with each other, the generation and recombination terms in the e–h continuity equations are non-zero only at the D–A interfacial nodes. Electron and hole transport are modeled by the drift-diffusion formalism. While the drift–diffusion equation cannot explicitly account for complex charge transport in polymeric crystals [33], most groups adopt this approach to explore the broad aspects of carrier transport within the OPV structures.

The boundary conditions for carrier densities at the metal–semiconductor contact are determined by the equilibrium carrier densities (defined by the metal work function, the HOMO and LUMO energy levels, and the corresponding effective density of states). Numerical values of all these parameters are tabulated in Table 5. Finally, we assume that the charge-density is low enough so that the Poisson equation need not be solved explicitly but can be approximated by a constant field defined by the built-in voltage ($V_{bi}$), applied voltage ($V$), and device thickness ($T_{film}$), i.e., $E=(V_{bi}-V)/T_{film}$. While the validity of the approximation can be easily established for relatively high mobility OPV cells, its application to very low mobility OPV devices requires additional care. We wish to mention explicitly that the transport model used in this paper follows Refs. [6,7]. We claim no new contribution to model development; rather, we use this well-known, well-calibrated, and well-tested process-device model to explore the implications of morphology on the efficiency of organic solar cells.

For a given OPV structure (Fig. 1(a–c)), we solve the coupled transport equations for excitons, electrons, and holes self-consistently at each bias condition to construct the current-voltage characteristics of the solar cell, see Fig. 1d. Based on the $J$–$V$ characteristics so generated, we calculate efficiency as well as other solar cell parameters such as short circuit current density, open circuit voltage, and FF. The short circuit current in the $J$–$V$ curve is defined as the current at the zero terminal voltage, i.e., $J_{SC}\equiv J(V=0)$, the open circuit voltage is defined as the terminal voltage for which current from the cell is zero, i.e., $V_{OC}\equiv V(J=0)$, and the FF is calculated by the formula $FF=J_mV_m/(J_{SC}V_{OC})$, where $J_m$ and $V_m$ are the current density and voltage at the maximum power point of the $J$–$V$ curve, respectively.

## 3. Results and discussion

With the model system described in the previous section, we now explore how the efficiency of a cell depends on its morphology. Although we choose typical values for the model parameters (see Tables 1 and 2) based on P3HT:PCBM system to illustrate our approach, the conclusions are general and should apply to a broad range of polymeric OPV.

### 3.1. Comparison of ordered and random BHJ cells

Let us first consider how the randomness of the OPV morphology affects the key device parameters such as efficiency, $J_{SC}$,$V_{OC}$, and $FF$. To quantify the structural randomness of OPV, we generate a series of three dimensional (3D) BHJ morphology for different anneal duration ($t_a$) and temperature ($T_a$); the details of process simulation are described in Ref. [6,7]. The initial condition ($t_a=0$) for simulating the morphology is a structure with random composition fluctuation around a mean composition value given by the mixing ratio of the D–A molecules. This random initial condition implies that even if the anneal duration and temperature are identical, the morphologies generated from different initial conditions will be structurally different. Thus, the randomness in OPV morphologies has two distinct sources: one comes from the initial/starting random composition and the other is from process variation ($t_a$, $T_a$).

In Fig. 2(a), we show the time evolution of BHJ morphology, simulated on a 3D domain of $100\times100\times100$ grid points with uniform grid spacing of 1 nm. Once the morphology is simulated, we characterize it by the average cluster size, $W$ (see Fig. 2a). The time evolution of $W$ is plotted in Fig. 2b. We also plot in Fig. 2c the evolution of the total D/A interfacial area of the simulated morphology. Each point in Figs. 2b and 2c represents a distinct

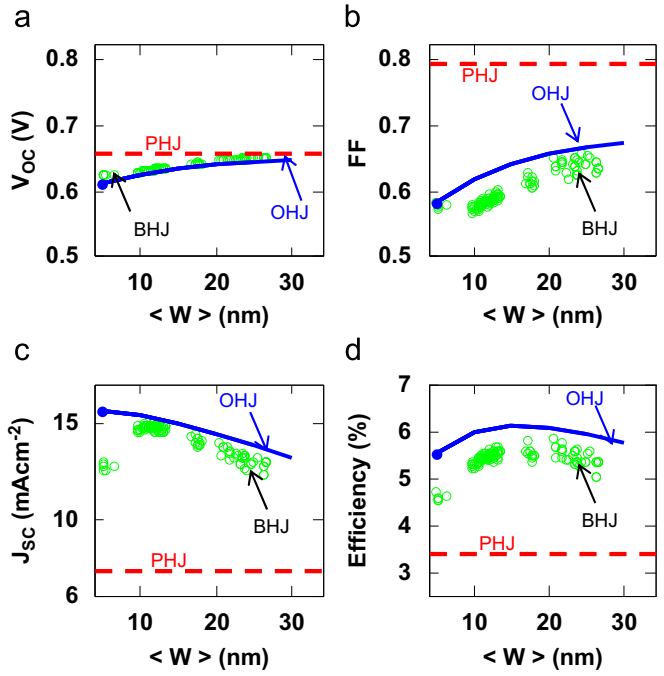


**Fig. 3.** Performance comparison of ordered heterojunction (OHJ, solid line), random bulk heterojunction (BHJ, symbols) and planar heterojunction (PHJ, dashed line) solar cell. The performance metrics are (a) open circuit voltage ($V_{OC}$), (b) fill factor (*FF*), (c) short circuit current density ($J_{SC}$), and (d) efficiency ($\eta$). Each scattered symbol corresponds to a particular random morphology (BHJ) with an average domain size $<W>$ (x-axis). (For interpretation of the references to colour in this figure legend, the reader is referred to the web version of this article).

morphology corresponding to the anneal duration shown in x-axis. The spread in the domain size (or interfacial area) for a given anneal duration reflects the randomness in the OPV morphology. For each of the simulated morphology, characterized by its domain width $W$, we calculate the $J$–$V$ characteristics by following the procedure described in section 2. From the $J$–$V$ characteristics, we compute all the solar cell performance metrics and plot them as a function of morphology-specific parameter $W$ as open circles in Fig. 3(a–d). The scatter of the points reflects randomness of the morphology resulting from initial conditions as well as fluctuation in anneal temperature, anneal time, etc. Generally speaking, we find that an optimized BHJ–OPV cell with the specified parameters (Tables 2–5) can achieve average efficiency of $\eta \sim 5.5\%$ with $J_{SC} \sim 14$ mA cm$^{-2}$, $V_{OC} \sim 0.62$ $V$, $FF \sim 0.63$.

Next, we define a series of ordered morphology (OHJ) with the domain width ($W$) and domain height equal to the film thickness (see Fig. 1c). Unlike the C–H process model for BHJ–OPV, these ordered OPV structures are created mechanically with fixed geometric dimensions. In practice, these structures could be fabricated by stamping or lithography [12,13]. We assume minority carrier blocking at both contacts. We calculate the $J$–$V$ characteristics of this series of ordered structures using exactly the same transport equations and boundary conditions as we did for the BHJ–OPV. Finally, we plot the corresponding quantities of $V_{OC}$, $FF$, $J_{SC}$, and efficiency as a function of $W$ as solid blue lines in Fig. 3(a–d). For completeness, we also plot the solar cell performance metrics for PHJ cell (dashed red lines) in Fig. 3(a–d).

How does the random OPV compare with the ordered OPV? First, among the PV parameters, the open circuit voltage is found least sensitive to morphology and is mainly determined by the material constants (see Fig. 3a). In Fig. 3a we plot $V_{OC}$ variation for random BHJ, OHJ, and PHJ cells, which shows that $V_{OC}$ value is almost same for all these morphologies. This insensitivity of $V_{OC}$ with geometry can be understood from the fact that both $J_{SC}$ and recombination current are proportional to the interfacial area [34]. Since $V_{OC}$ is determined by the ratio of these two currents, the interfacial area dependence cancels out and $V_{OC}$ becomes insensitive to morphology (detailed discussion on the insensitivity of $V_{OC}$ is given in Ref.[7]).

Second, the fill-factors calculated from numerical simulation for both ordered and random morphologies are close and vary in the range of 0.55–0.65. The experimentally reported $FF^{BHJ}$ values for P3HT:PCBM based BHJ cells are slightly lower compared to the simulation, typically in the range of $\sim$0.5–0.6 [35]. It is interesting that these FFs are much lower than that of PHJ cell ($FF^{PHJ} \sim .8$ in Fig. 3b). There are many experimental evidences for this higher FF of PHJ cells, where typically $FF^{PHJ}$ is measured in the range of $\sim$ (0.6–0.7) [36]. Although specific values are slightly different, our conclusion of higher $FF$ for PHJ geometry compared to the random BHJ/OHJ structures is broadly consistent with experiment. We attribute the lower $FF$ of BHJ/OHJ cells to the higher *intrinsic* series resistance associated with the percolating paths of the device. Among the various OPV structures, the average carrier extraction length in PHJ is the lowest and hence it offers the lowest *intrinsic* series resistance, which makes its $FF$ higher than BHJ/OHJ OPV especially for high-mobility materials.

Third, we find that the real advantage of OHJ morphology over the random BHJ structures lies in the enhancement of short circuit current density (see Fig. 3c) for smaller $W$ (or early anneal phase). More fundamentally, this higher $J_{SC}$ of ordered cells for lower $W$ arises from the fact that the ordered morphology operates above the percolation threshold for all domain width $W$ and volume ratio of the polymers, see Fig. 1c. Thus, the generated charge carriers always find continuous pathways for coming out of the cell. For random BHJ cells, at the early phase of annealing (this corresponds to the lower value of $W$ in Fig. 3), the active layer contains large number of floating islands of D/A phases and the heterointerfaces between the D–A regions are not well formed. Hence $J_{SC}$ of BHJ cells is lower compared to OHJ cells for smaller $W$ as shown in Fig. 3c (detailed discussion of annealing effect on the $J_{SC}$ of BHJ cell is given in [7]). With the increase in domain size $W$ (late annealing phase), the interfaces form sharp heterojunction and the floating islands in the active layer disappear by merging into percolating paths between the electrodes. Given the optimum 1:1 D-A mixing ratio (by volume), both the donor and acceptor phase volumes exceed the 3D site percolation threshold of $\sim$31%. It is well known that for such conditions, the donor and acceptors belong to their respective percolation clusters and there are very few isolated floating islands in the morphology. Thus, $J_{SC}$ of BHJ cells approaches the corresponding value of OHJ cells for larger $W$ (or late annealing phase).

Since $V_{OC}$ and FF of both OHJ and BHJ cells are similar, the efficiency comparison follows the analogous trend of $J_{SC}$, as shown in Fig. 3d. The figure clearly shows that efficiency of random BHJ cells is very close to that of perfectly ordered (ideal) structures. Thus, the plot confirms that there is no fundamental limitation related to morphology arising from the inexpensive solution-based processing of BHJ cells, provided that the process variables such as mixing ratio, anneal temperature, anneal duration, etc. have been chosen optimally.

Finally, we analyze the performance variability of random BHJ cell for a series of 3D morphologies. Fig. 3d might suggest that the efficiency of the random BHJ cells could vary considerably ($\sim$1% in absolute terms) depending on the cluster size and structural randomness. This variability in efficiency is mainly due to the structural randomness originated from the initial composition. However, we find that the scatter in efficiency reflects finite size of the simulation domain, i.e., 100 nm $\times$ 100 nm $\times$ 100 nm. In supplementary material, we plot the efficiency variation for the structures with the same thickness but increasing area to show that

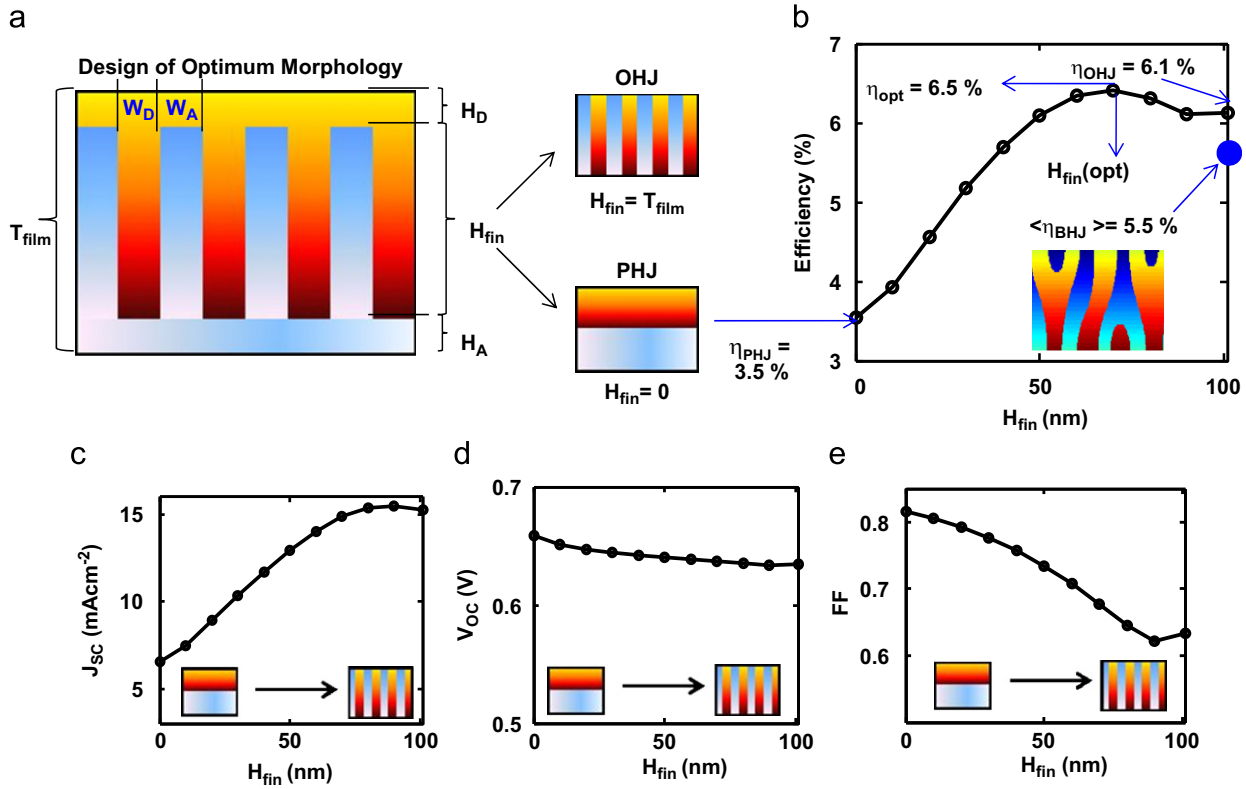


**Fig. 4.** Design rules for fabricating the optimum morphology (FIN–OPV). (a) The structure of the optimum morphology. For $H_{fin}=0$ the structure corresponds to PHJ cell and for $H_{fin}=T_{film}$, it is an OHJ. (b) Efficiency variation of FIN-OPV is plotted for the various fin heights. The fin width is kept fixed to the value of $W_{fin}=L_{ex}$. We find optimum fin height to be $H_{fin}(opt)\sim T_{flim}-\xi L_{ex}$, where $\xi$ is a number in the range $(1<\xi<2)$. The variation of other solar cell performance metrics, i.e., $J_{SC}$, $V_{OC}$, and *FF* are plotted in (c), (d), (e), respectively.

the spread in efficiency decreases monotonically with larger cell area. Thus, even for the smallest practical device dimensions (e.g., 1 mm × 1 mm × 100 nm), such spread in efficiency disappears and only the mean efficiency will be realized. *Hence the main conclusion of this study is that the inherent structural randomness of BHJ cells is not a concern for the performance variability of BHJ–OPVs.* It is important to note that a 2D analysis of such geometrical randomness overestimates the performance variability of BHJ–OPV [37], because the 2D percolation threshold of 50% incorrectly suggests significant number of floating islands even for 1:1 mixing ratio (by volume). However, for the large area cells (fabricated by roll-to-roll or other technique), there will be extrinsic variation in process parameters such as anneal temperature, mixing ratio, etc., which will lead to variation in average cluster size $W$ (and hence efficiency) among the cells. This extrinsic process variation might induce significant performance variability even for a large area cells. Other sources for variability in performance can arise from metal deposition and shunt formation [38], variability in the thickness of the blocking layers, etc. Thus, performance variability for BHJ cells remains a significant concern for achieving higher panel/module efficiency, even though our analysis shows that *intrinsic* morphological randomness does not contribute to this variability.

### 3.2. Design rules for optimum morphology

In this section, we explore the theoretical optimum morphology of OPV cells for the same set of transport parameters discussed in the previous section (see Table 2). The discussion in the previous section clearly indicates that it is difficult to improve $J_{SC}$ and $V_{OC}$ by engineering morphology, because $V_{OC}$ is morphology insensitive and $J_{SC}$ is almost optimal for average domain width $W\sim L_{ex}$. Thus, *FF* is the only parameter through which efficiency can be enhanced by morphology engineering. In Fig. 4a we show an interpenetrating fin like structure (Fin-OPV), which optimizes the *FF* without affecting the $V_{OC}$ and $J_{SC}$ and thus maximizes the OPV efficiency. However, the dimensions of the Fin-OPV need to be optimized as a function of the transport parameters such as exciton diffusion length, mobility and the recombination strength.

As shown in the Fig. 4a, the Fin-OPV has four independent geometrical dimensions, namely, the donor fin width ($W_D$), acceptor fin width ($W_A$), donor offset height ($H_D$) and acceptor offset height ($H_A$). For simplicity, we assume the structure is symmetric with equal volume of donor and acceptor material, so that $W_A=W_D=W_{fin}$ and $H_A=H_D=(T_{flim}-H_{fin})/2$, with two independent variables of fin height ($H_{fin}$) and fin width ($W_{fin}$) available for optimization. The general problem of optimizing partially ordered OPV with unequal volume fraction is left as an open problem for future work.

The proposed fin-like morphology in Fig. 4a unifies both the PHJ ($H_{fin}=0$) and the fully ordered ($H_{fin}=T_{flim}$) structure within a common geometrical construct. The reason for the existence of an optimum fin height is as follows: the PHJ structure is excellent for charge carrier transport, but has a very poor efficiency for exciton collection. On the other hand, the ordered BHJ collects almost all the excitons, but the large surface area increases interface recombination and longer carrier extraction length increases 'series' resistance, therefore, the structure is non-optimal for the charge transport. The fin-like morphology balances the two desirable properties of OPV: excellent carrier transport in the PHJ cell and the exciton collection property of ordered cell. In Fig. 4b, we plot the efficiency of FIN–OPV as a function of fin height. The figure clearly shows that the maximum efficiency is close to $\eta_{max}\sim 6.5\%$, corresponding to $H_{fin}(opt)\sim 75$ nm. The optimum fin dimension and the corresponding efficiency depend on material parameters such as mobility and recombination

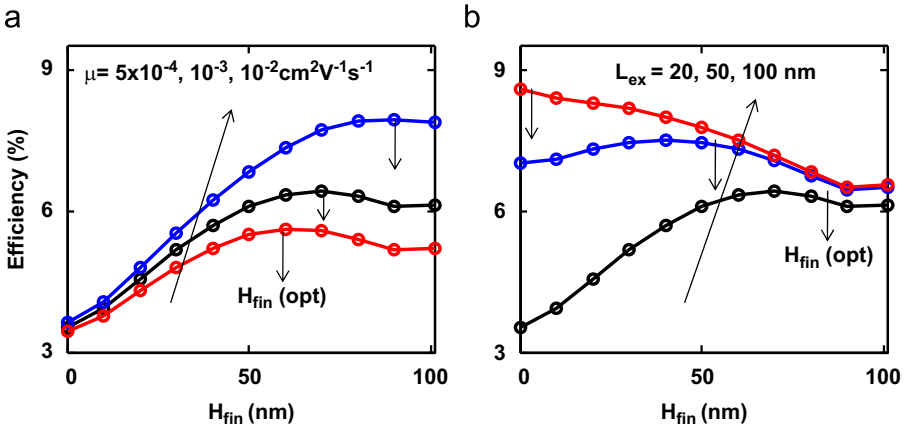


**Fig. 5.** Variation of optimum fin-height (of the Fin-OPV) with improved transport parameters. (a) Effect of carrier mobility and (b) effect of exciton diffusion length.

constant at the interface. In general, $H_{fin}(opt) \sim T_{flim} - \xi L_{ex}$ where $\xi$ is a number in the range $(1 < \xi < 2)$ depending on the values of the transport parameters such as $L_{ex}$, $\mu$, and $\gamma$ (typical values are given in Table 2). The choice of $W$ depends primarily on the efficient exciton collection, which is guaranteed if $W_{fin} \sim L_{ex}$, consistent with results in Fig. 3d. Given the transport parameters, the PHJ OPVs ($\eta \sim 3.5\%$) are far from optimal, a well known result for traditional material systems [36].

### 3.3. *Efficiency projection with improved material parameters*

In this section, we extend the efficiency analysis by exploring the impact of the transport parameters on the optimum design of Fin-OPV. In Fig. 5a, we study the effect of mobility improvement on the optimum fin height (other transport parameters are kept same at typical values). We find that improvement in mobility has a significant effect on the efficiency of OHJ/BHJ structure, whereas it has very little effect on the PHJ geometry. The figure shows that with improved mobility, the optimum fin height approaches the film thickness, i.e., OHJ. This is easily understood because increasing fin-height improves exciton collection, while the high mobility ensures that the FF is not compromised.

In Fig. 5b, we study the effect of excition diffusion length on the optimum fin height ($H_{fin}$), and we find that $H_{fin}(opt)$ reduces with higher value of $L_{ex}$. This is an intuitive result: with higher value of $L_{ex}$ (comparable to donor layer thickness), all the photo-generated excitons are collected irrespective of the fin height. Since lower fin height improves the fill factor (Fig. 4e), a optimum morphology with higher $L_{ex}$ should have lower $H_{fin}$. In fact, $L_{ex}$ is a real bottleneck for PHJ cells, where the exciton collection volume is limited by $L_{ex}$. For OHJ or BHJ cell, once $L_{ex}$ exceeds the domain width $W$, no further improvement in exciton collection (and hence efficiency) is possible. Hence in Fig. 5b, we find that $L_{ex}$ affects PHJ cell efficiency significantly, while it has very little effect on the ordered BHJ structure.

Finally, we explore the efficiency limits of OPV with respect to improved mobility. A number of recent publications have suggested the possibility of enhancing the mobility by increasing the nano-scale crystallinity and molecular packing of the polymer film [39,40]. Silva et al. have shown that 'doping' of polymers by carbon nanotubes can enhance carrier extraction rate by improving the effective carrier mobility [41] in the film. Thus, it is important to study the effect of the improved mobility on the efficiency gain/limits of OPV cells with different morphologies. In Fig. 6a, we plot the efficiency enhancement for both PHJ and OHJ cells with improved mobility. The corresponding performance metrics, i.e., $J_{SC}$, $V_{OC}$, and *FF* are also plotted in Fig. 6(b–d). Remarkably, we find

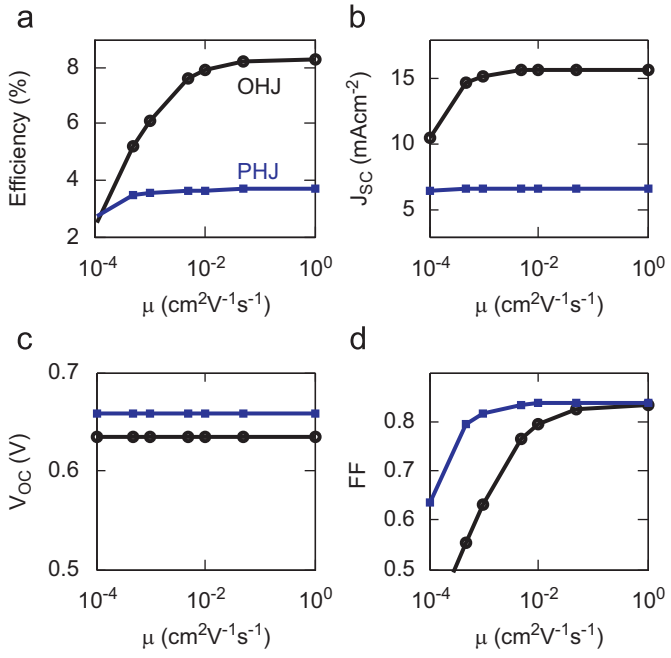


**Fig. 6.** Effect of improved carrier mobility on various solar cell performance metrics: (a) efficiency ($\eta$), (b) short circuit current density ($J_{SC}$), (c) open circuit density voltage ($V_{OC}$), and (d) fill factor (*FF*).

that increasing material mobility improves the efficiency to ~8%. However, beyond a critical value of $\mu \sim 10^{-2}$ cm$^2$ V$^{-1}$ s$^{-1}$, further improvement in mobility is not reflected in higher efficiency of the cell. The initial improvement in efficiency with high carrier mobility can be traced to the significant improvement in *FF*, see Fig. 6d. Since the *FF* improvement saturates to a value of 85% with $\mu \sim 10^{-2}$ cm$^2$ V$^{-1}$ s$^{-1}$, any further improvement in mobility does not increase the cell efficiency. However, the current material systems have $\mu \sim 10^{-4}$–$10^{-3}$ cm$^2$ V$^{-1}$ s$^{-1}$, with the corresponding *FF* of 0.4–0.6 [35]. Therefore, improvement in mobility is still an important research objective for achieving higher *FF* and cell efficiency.

## 4. Conclusion

In this paper, we show that the efficiency of the solution-processed BHJ cells (with random morphology) is very close to

the perfectly ordered structures, which suggests that the inexpensive solution based processing of BHJ cells imposes no inherent limitation on the cell efficiency (associated with morphology) compared to the ordered OPV cells fabricated by more expensive techniques. We also show that the inherent structural randomness of solution-processed BHJ cells is not a concern for the performance variability of large-area cells. However, precise control of process variables remains a significant concern for extrinsic performance variability of OPV. Finally, we explore the problem of optimal morphology as a function of material parameters. We find that the optimal morphology resembles the interpenetrating fin-like architecture with the exact dimensions optimized for a given set of transport parameters. These results establish the future prospects and fundamental limits of performance gain that can be obtained by tailoring the morphology of a given pair of D/A material systems.

## Acknowledgment

This material is based upon work supported as part of the Center for Re-Defining Photovoltaic Efficiency Through Molecule Scale Control, an Energy Frontier Research Center funded by the U.S. Department of Energy, Office of Science, Office of Basic Energy Sciences under Award Number DE-SC0001085.The computational resources for this work were provided by the Network of Computational Nanotechnology under NSF Award EEC-0228390.

## Appendix A

(See Tables 1–5 for more details)

**Table 1**
Summary of model equations.

**Equations for process model:**
Free energy of mixing:

$$f_{\mathrm{mix}} = \frac{k_B T_a}{\nu_{\mathrm{site}}}\left[\frac{\phi \ln(\phi)}{N_D} + \frac{(1-\phi)\ln(1-\phi)}{N_A} + \chi\phi(1-\phi)\right] \quad (1)$$

Cahn–Hilliard (C–H) equation:

$$\frac{\partial \phi}{\partial t_a} = M_0\left(\nabla^2 \frac{\partial f_{\mathrm{mix}}}{\partial \phi} - 2\kappa\nabla^4\phi\right) \quad (2)$$

**Equations for exciton transport:**
Exciton continuity equation:

$$D_{\mathrm{ex}}\nabla^2 n_{\mathrm{ex}} = G_{\mathrm{ex}}(x,y,z) - R_{\mathrm{ex}}(n_{\mathrm{ex}}) \quad (3)$$

$$R_{\mathrm{ex}} = \frac{n_{\mathrm{ex}}}{\tau_{\mathrm{ex}}}; G_{\mathrm{ex}} = uniform(assumption) \quad (4)$$

**Equations for charged carrier transport:**
Poisson equation:

$$\nabla(\epsilon_r\epsilon_0\nabla\psi) = -q(n_h - n_e) \quad (5)$$

Continuity equation:

$$\nabla J_{e,h} = \mp\left(G_{e,h}(n_{\mathrm{ex}}) - R_{e,h}(n_e, n_h)\right) \quad (6)$$

Drift-diffusion equation:

$$J_{e,h} = \mu_{e,h} n_{e,h}(-\nabla\psi) \pm D_{e,h}\nabla n_{e,h} \quad (7)$$

Recombination equation:

$$R_{e,h}(n_e, n_h) = \gamma(n_e, n_h - n_{\mathrm{int}}^2) \quad (8)$$

Electron boundary condition:

$$\nabla n_e\big|_{z=0} = 0; n_e(z = T_{\mathrm{film}}) = N_c\ exp\left(-\frac{\Phi_c - LUMO_A}{kT}\right) \quad (9)$$

Hole boundary condition:

$$n_h(z=0) = N_v\ \exp\left(-\frac{\Phi_a - HOMO_D}{kT}\right); \nabla n_h\big|_{z=T_{\mathrm{film}}} = 0 \quad (10)$$

**Table 2**
Process simulation parameters and variables (see Eqs. (1) and (2) in Table 1).

| Parameter | Symbol | Numerical values/units | Description |
|---|---|---|---|
| Composition | $\phi$ | (0–1) | This the composition variable which defines the morphology. |
| Anneal temperature | $T_a$ | 393 K | The temperature at which the phase segregation takes place |
| Anneal time | $t_a$ | s | This the independent variable in the process model, representing the anneal duration. |
| Flory parameter | $\chi$ | Depends on $T_a$ A representative value of 0.09 is used in simulation | This is interaction parameter between the donor and the acceptor molecules [23,24]. For PS/PMMA polymeric system , $\chi \sim (0–0.1)$. |
| Gradient energy coefficient | $\kappa$ | $10^{-11}\ J/m$ | It characterize the energy contribution due to the formation of diffused interface [23]. |
| Effective mobility | $M_0$ | $10^{-26}\mathrm{m}^5\mathrm{J}^{-1}\mathrm{s}^{-1}$ | This the diffusive mobility of the organic molecules in the mixture [23]. |
| Donor volume fraction | $\eta_D$ | 0.5 | It is same as the mixing ratio of the donor acceptor molecules. |
| Volume of the reference site | $\nu_{\mathrm{site}}$ | $10^{-29}\ \mathrm{m}^3$ | This is the reference volume in the Flory–Huggins lattice model. |
| Size of Donor molecules | $N_D$ | 33 | This is the relative size of the organic molecule (donor). |
| Size of acceptor molecules | $N_A$ | 33 | This is the relative size of the organic molecule (acceptor). |
| Free energy of mixing | $f_{\mathrm{mix}}$ | $\mathrm{J/m}^3$ | This is the free energy density function describing the entropy and enthalpy of the mixture. |

**Table 3**
Exciton transport parameters (see Eqs. (3–4) in Table 1).

| Parameter | Symbol | Numerical values/units | Description |
|---|---|---|---|
| Exciton recombination time | $\tau_{ex}$ | 1 ns | Exciton recombination time. |
| Exciton diffusion coefficient | $D_{ex}$ | $10^{-7}$ cm$^2$/s | Effective diffusion coefficient for the exciton transport. |
| Exciton diffusion length | $L_{ex}=\sqrt{D_{ex}\tau_{ex}}$ | 10 nm | This is the diffusion length, the photo-generated excitons travel in its lifetime. |
| Exciton recombination rate | $R_{ex}$ | cm$^{-3}$s$^{-1}$ | This is a position dependent variable representing exciton self-recombination rate. |
| Exciton generation rate | $G_{ex}$ | cm$^{-3}$s$^{-1}$ | This is a position dependent variable representing exciton generation rate. |
| Exciton concentration | $n_{ex}$ | cm$^{-3}$ | This is a position dependent variable representing the steady state exciton density. |

**Table 4**
Charged carrier transport parameters (see Eqs. (5–8) in Table 1).

| Parameter | Symbol | Numerical values/ units | Description |
|---|---|---|---|
| Charge of an electron | $q$ | $1.6\times10^{-19}$ C | Charge of an electron |
| Carrier mobility ('e' stands for electron and 'h' for holes) | $\mu_{e,h}$ | $\mu_e=10^{-3}$ cm$^2$ V$^{-1}$ s$^{-1}$<br>$\mu_h=10^{-4}$ cm$^2$ V$^{-1}$ s$^{-1}$ | Mobility of electrons in the acceptor material and mobility of holes in the donor material. |
| Carrier diffusion coefficient | $D_{e,h}$ | $\frac{k_bT}{q}\mu_{e,h}$ | Diffusion coefficients of electron and holes in acceptor and donor respectively. Electronic charge is '$q$', $k_b$ is the Boltzmann constant, and $T$ is temperature. |
| Bimolecular based interfacial recombination strength | $\gamma$ | ($10^{-9}$–$10^{-11}$) cm$^3$/s | This is the bimolecular recombination strength. Carrier recombination takes place only at the donor–acceptor interface. |
| Intrinsic carrier density at the D–A interface | $n_{int}$ | $10^{11}$cm$^{-3}$ | This is the intrinsic carrier density at the donor-acceptor interface in the active material. |
| Relative permittivity | $\epsilon_r$ | 3–4 | This is the relative permittivity of the organic materials. |
| Electro static potential | $\psi$ | V | This is the electrostatic potential inside the solar cell. |
| Carrier concentration | $n_{e,h}$ | cm$^{-3}$ | This is a position dependent variable representing the e/h density. Generally, electrons flow in the acceptor and holes flow in donor. |
| Carrier recombination rate ('e' stands for electron and 'h' for holes) | $R_{e,h}$ | cm$^{-3}$s$^{-1}$ | This is a position dependent variable representing e/h recombination rate. e/h recombination takes place only at the interface. |
| Carrier generation rate | $G_{e,h}$ | cm$^{-3}$s$^{-1}$ | This is a position dependent variable representing e/h generation rate. e/h generation takes place only at the interface. |
| Current density | $J_{e,h}$ | A/cm$^2$ | This is a position dependent variable representing e/h current density. Electron current flows in acceptor and hole current in donor. |

**Table 5**
Boundary condition parameters for the electron–hole densities at the electrode–semiconductor interface (see Eqs. (9–10) in Table 1).

| Parameter | Symbol | Numerical values/units | Description |
|---|---|---|---|
| Lowest unoccupied molecular orbital (Donor) | $LUMO_D$ | 3.0 eV | The chosen numerical values is for P3HT. |
| Highest occupied molecular orbital (Donor) | $HOMO_D$ | 4.9 eV | The chosen numerical values is for P3HT. |
| Lowest unoccupied molecular orbital (Acceptor) | $LUMO_A$ | 3.7 eV | The chosen numerical values is for PCBM. |
| Highest occupied molecular orbital (Acceptor) | $HOMO_A$ | 6.1 eV | The chosen numerical values is for PCBM. |
| Effective density of states ($HOMO_D$,$HOMO_A$,$LUMO_D$,$LUMO_A$) | $N_C$,$N_v$ | $10^{21}$ cm$^{-3}$ | Number of energy states available for electron/holes, at the LUMO/HOMO. |
| Cathode work function (Al) | $\Phi_c$ | 3.9 eV | The chosen numerical values is for Al. |
| Anode work function (ITO) | $\Phi_a$ | 4.7 eV | The chosen numerical values is for ITO. |

## Appendix B. Supplementary material

Supplementary data associated with this article can be found in the online version at doi:10.1016/j.solmat.2011.11.042.

## References


[1] C.W. Tang, Two-layer organic photovoltaic cell, Appl. Phys. Lett. 48 (1986) 183–185.
[2] 〈http://www.solarmer.com/, http://www.solarmer.com/〉, (n.d.).
[3] G. Yu, J. Gao, J.C. Hummelen, F. Wudl, A.J. Heeger, Polymer photovoltaic cells: enhanced efficiencies via a network of internal donor–acceptor heterojunctions, Science 270 (1995) 1789–1791.
[4] R.A. Street, M. Schoendorf, A. Roy, J.H. Lee, Interface state recombination in organic solar cells, Phys. Rev. B. 81 (2010) 205307.
[5] S.H. Park, A. Roy, S. Beaupre, S. Cho, N. Coates, J.S. Moon, et al., Bulk heterojunction solar cells with internal quantum efficiency approaching 100%, Nat. Photon. 3 (2009) 297–302.
[6] G.A. Buxton, N. Clarke, Predicting structure and property relations in polymeric photovoltaic devices, Phys. Rev. B. 74 (2006) 085207.
[7] B. Ray, P.R. Nair, M.A. Alam, Annealing dependent performance of organic bulk-heterojunction solar cells: a theoretical perspective, Sol. Energy Mater. Sol. Cells. (2011);
B. Ray, M.S. Lundstrom, M.A. Alam, Can morphology tailoring improve the open circuit voltage of organic solar cell, Appl. Phys. Lett., in press.
[8] B. Lei, Y. Yao, A. Kumar, Y. Yang, V. Ozolins, Quantifying the relation between the morphology and performance of polymer solar cells using Monte Carlo simulations, J. Appl. Phys. 104 (2008) 024504–024506.
[9] K. Maturova´, S.S. van Bavel, M.M. Wienk, R.A.J. Janssen, M. Kemerink, Morphological device model for organic bulk-heterojunction solar cells, Nano Lett. 9 (2009) 3032–3037.

[10] M. Shah, V. Ganesan, Correlations between morphologies and photovoltaic properties of Rod – Coil block copolymers, Macromolecules 43 (2010) 543–552.
[11] A.A. Gorodetsky, C.Y. Chiu, T. Schiros, M. Palma, M. Cox, Z. Jia, et al., Reticulated heterojunctions for photovoltaic devices, Angew. Chem. Int. Ed. 49 (2010) 7909–7912.
[12] Z. Fan, H. Razavi, J. won Do, A. Moriwaki, O. Ergen, Y.L. Chueh, et al., Three-dimensional nanopillar-array photovoltaics on low-cost and flexible substrates, Nat. Mater. 8 (2009) 648–653.
[13] M.D. McGehee, Nanostructured organic-inorganic hybrid solar cells, MRS Bull. 34 (2009) 95–100.
[14] J.A. Renz, T. Keller, M. Schneider, S. Shokhovets, K.D. Jandt, G. Gobsch, et al., Multiparametric optimization of polymer solar cells: a route to reproducible high efficiency, Sol. Energy Mater. Sol. Cells 93 (2009) 508–513.
[15] F.C. Krebs, Fabrication and processing of polymer solar cells: a review of printing and coating techniques, Sol. Energy Mater. Sol. Cells 93 (2009) 394–412.
[16] L. Zeng, C.W. Tang, S.H. Chen, Effects of active layer thickness and thermal annealing on polythiophene: fullerene bulk heterojunction photovoltaic devices, Appl. Phys. Lett. 97 (2010) 053305-3.
[17] Byung-Kwan Yu, Doojin Vak, Jang Jo, Seok-In Na, Seok-Soon Kim, Mi-Kyoung Kim, et al., Factors to be considered in bulk heterojunction polymer solar cells fabricated by the spray process, IEEE J. Sel. Top. Quantum Electron. 16 (2010) 1838–1846.
[18] F.C. Krebs, S.A. Gevorgyan, B. Gholamkhass, S. Holdcroft, C. Schlenker, M.E. Thompson, et al., A round robin study of flexible large-area roll-to-roll processed polymer solar cell modules, Sol. Energy Mater. Sol. Cells 93 (2009) 1968–1977;
S. Dongaonkar, Y. Karthik, S. Mahapatra, M. Alam, The physics of shadow degradation in thin film solar cell, in: Proceedings of International Reliability Physics Symposium Monterey, CA, USA, 2011, pp. 557–561;
M.A. Alam, S. Dongaonkar, Y. Karthik, S. Mahapatra, Intrinsic reliability of amorphous silicon thin film solar cells, in: Proceedings of International Reliability Physics Symposium Anaheim, CA, USA, 2010, pp. 312–317.
[19] J. Kim, K. Kim, S. Hwan, Ko, W. Kim, Optimum design of ordered bulk heterojunction organic photovoltaics, Sol. Energy Mater. Sol. Cells 95 (2011) 3021–3024.
[20] C.M. Martin, V.M. Burlakov, H.E. Assender, D.A. Barkhouse, A numerical model for explaining the role of the interface morphology in composite solar cells, J. Appl. Phys. 102 (2007) 104506.
[21] E. Krali, R.J. Curry, Optimization of hybrid organic–inorganic interdigitated photovoltaic device structure using a 2D diffusion model, ACS Nano 5 (2011) 3069–3078.
[22] P.G. de Gennes, Dynamics of fluctuations and spinodal decomposition in polymer blends, J. Chem. Phys. 72 (1980) 4756–4763.
[23] Y. Shang, D. Kazmer, M. Wei, J. Mead, C. Barry, Numerical simulation of phase separation of immiscible polymer blends on a heterogeneously functionalized substrate, J. Chem. Phys. 128 (2008) 224909-7.
[24] J. Kressler, N. Higashida, K. Shimomai, T. Inoue, T. Ougizawa, Temperature dependence of the interaction parameter between polystyrene and poly(-methyl methacrylate), Macromolecules 27 (1994) 2448–2453.
[25] J. Jo, S.S. Kim, S.-I. Na, B.K. Yu, D.Y. Kim, Time-dependent morphology evolution by annealing processes on polymer: fullerene blend solar cells, Adv. Funct. Mater. 19 (2009) 866–874.
[26] V.S. Gevaerts, L.J.A. Koster, M.M. Wienk, R.A.J. Janssen, Discriminating between bilayer and bulk heterojunction polymer: fullerene solar cells using the external quantum efficiency, ACS Appl. Mater. Interfaces 0 (2011).
[27] F. Monestier, J.J. Simon, P. Torchio, L. Escoubas, F. Flory, S. Bailly, et al., Modeling the short-circuit current density of polymer solar cells based on P3HT:PCBM blend, Sol. Energy Mater. Sol. Cells 91 (2007) 405–410.
[28] R.A. Street, S. Cowan, A.J. Heeger, Experimental test for geminate recombination applied to organic solar cells, Phys. Rev. B. 82 (2010) 121301.
[29] R. Mauer, I.A. Howard, F. Laquai, Effect of nongeminate recombination on fill factor in polythiophene/methanofullerene organic solar cells, J. Phys. Chem. Lett. 1 (2010) 3500–3505.
[30] T.M. Clarke, J.R. Durrant, Charge photogeneration in organic solar cells, Chem. Rev. 110 (2010) 6736–6767.
[31] L.J. Koster, V.D. Mihailetchi, P.W. Blom, Bimolecular recombination in polymer/fullerene bulk heterojunction solar cells, Appl. Phys. Lett. 88 (2006) 052104.
[32] R.C.I. MacKenzie, T. Kirchartz, G.F.A. Dibb, J. Nelson, Modeling nongeminate recombination in P3HT:PCBM solar cells, J. Phys. Chem. C 115 (2011) 9806–9813.
[33] K.O. Sylvester-Hvid, S. Rettrup, M.A. Ratner, Two-dimensional model for polymer-based photovoltaic cells: numerical simulations of morphology effects, J. Phys. Chem. B 108 (2004) 4296–4307.
[34] B. Ray, M.A. Alam, A compact physical model for morphology induced intrinsic degradation of organic bulk heterojunction solar cell, Appl. Phys. Lett. 99 (2011) 033303-033303.
[35] D. Gupta, S. Mukhopadhyay, K.S. Narayan, Fill factor in organic solar cells, Sol. Energy Mater. Sol. Cells 94 (2010) 1309–1313.
[36] A.L. Ayzner, C.J. Tassone, S.H. Tolbert, B.J. Schwartz, Reappraising the need for bulk heterojunctions in polymer – fullerene photovoltaics: the role of carrier transport in all-solution-processed P3HT/PCBM bilayer solar cells, J. Phys. Chem. C 113 (2009) 20050–20060.
[37] B. Ray, M.A. Alam, Optimum Morphology and Performance Gains of Organic Solar Cells, In: 37th IEEE Photovoltaic Specialists Conference, IEEE, Seattle, WA, 2011.
[38] S. Dongaonkar, J.D. Servaites, G.M. Ford, S. Loser, J. Moore, R.M. Gelfand, et al., Universality of non-Ohmic shunt leakage in thin-film solar cells, J. Appl. Phys. 108 (2010) 124509.
[39] L. Li, W. Hu, H. Fuchs, L. Chi, Controlling molecular packing for charge transport in organic thin films, Adv. Energy Mater. 1 (2011) 188–193.
[40] C.-W. Chu, H. Yang, W.-J. Hou, J. Huang, G. Li, Y. Yang, Control of the nanoscale crystallinity and phase separation in polymer solar cells, Appl. Phys. Lett. (2008).
[41] A.J. Miller, R.A. Hatton, S.R.P. Silva, Interpenetrating multiwall carbon nanotube electrodes for organic solar cells, Appl. Phys. Lett. 89 (2006) 133117-3.